Electronic Supplementary Material (ESI) for Journal of Materials Chemistry A.

Electronic Supplementary Information

Setaria-Inflorescence-Structured Catalyst Based on Nickel-Cobalt Wrapped Silver Nanowire Conductive Networks for Highly Efficient Hydrogen Evolution

Kailing Zhou,[a] Qianqian Zhang,*[a] Zelin Wang,[b] Changhao Wang,[a] Changbao Han,[a] Xiaoxing Ke,[b] Zilong Zheng,[a] Hao Wang,*[a] Jingbing Liu [a] and Hui Yan [a]

[a] College of Materials Science and Engineering, Beijing University of Technology, Beijing 100124, P. R. China. E-mail: zhangqianqian@bjut.edu.cn; haowang@bjut.edu.cn

[b] Institute of Microstructure and Properties of Advanced Materials, Beijing University of Technology, Beijing 100124, P. R. China.

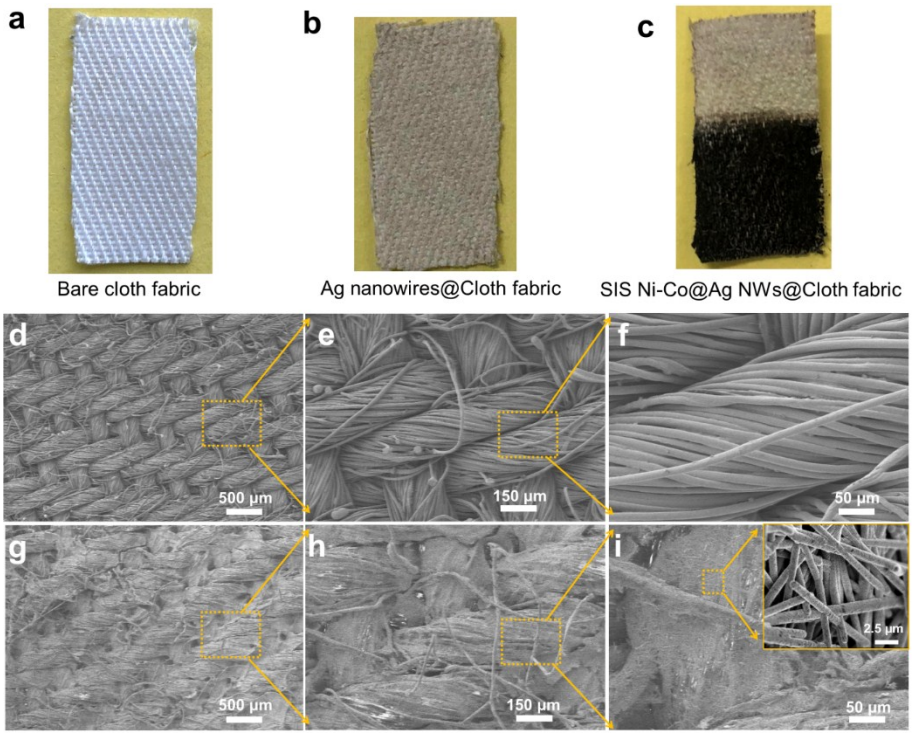

Figure S1. The the digital images of a) bare carbon fabric, b) the Ag nanowires supported on cloth fabric and c) the as-prepared SIS Ni-Co@Ag nanowires network on cloth fabric. The different-magnification SEM images of d-f) bare cloth fabric substrate and g-i) The fabricated SIS Ni-Co@Ag nanowires on cloth fabric substrate.

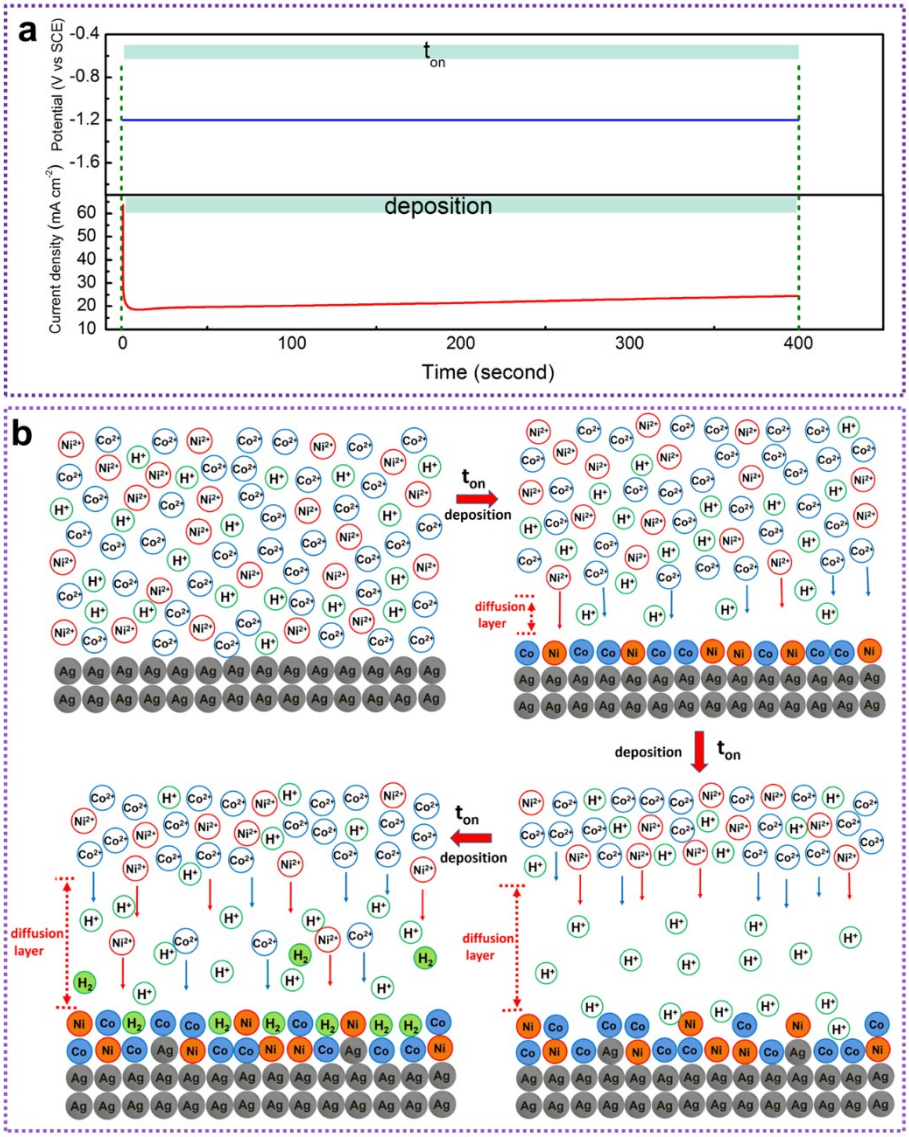

Figure S2. a) The potentiostatic electrodeposition model and b) simplified electrochemical reaction mechanism for fabricating the Setaria-inflorescence-structured Ni-Co@Ag nanowires.

During the electrodeposition process, the Co and Ni metals are formed simultaneously from an aqueous precursor electrolyte without order. At the beginning of potentiostatic model electrodeposition process (Figure S2a), there is a high concentration of Co^{2+} and Ni^{2+} metal ions near the deposition interface, and almost every active site is filled with metal ions (Figure S2b). After a short reaction process (Step (1)), metal ions near the deposition interface are exhausted with decreasing ion concentration, and a thin ions diffusion layer is produced. The thickness of the diffusion layer will further increase with the prolonging of deposition process (Step (2)).[1] Consequently, the metal ions need to take time to cross through the diffusion layer to participate in electrodeposition reaction. The high rate of electrodeposition than the rate of metal ion transport will cause the hydrogen evolution due to the high cathodic deposition

potential (-1.2 V vs SCE) in an aqueous solution (Step (3)).[2] The hydrogen evolution will serve as a dynamic template for fabricating nanochannels Ni-Co layer.[3]

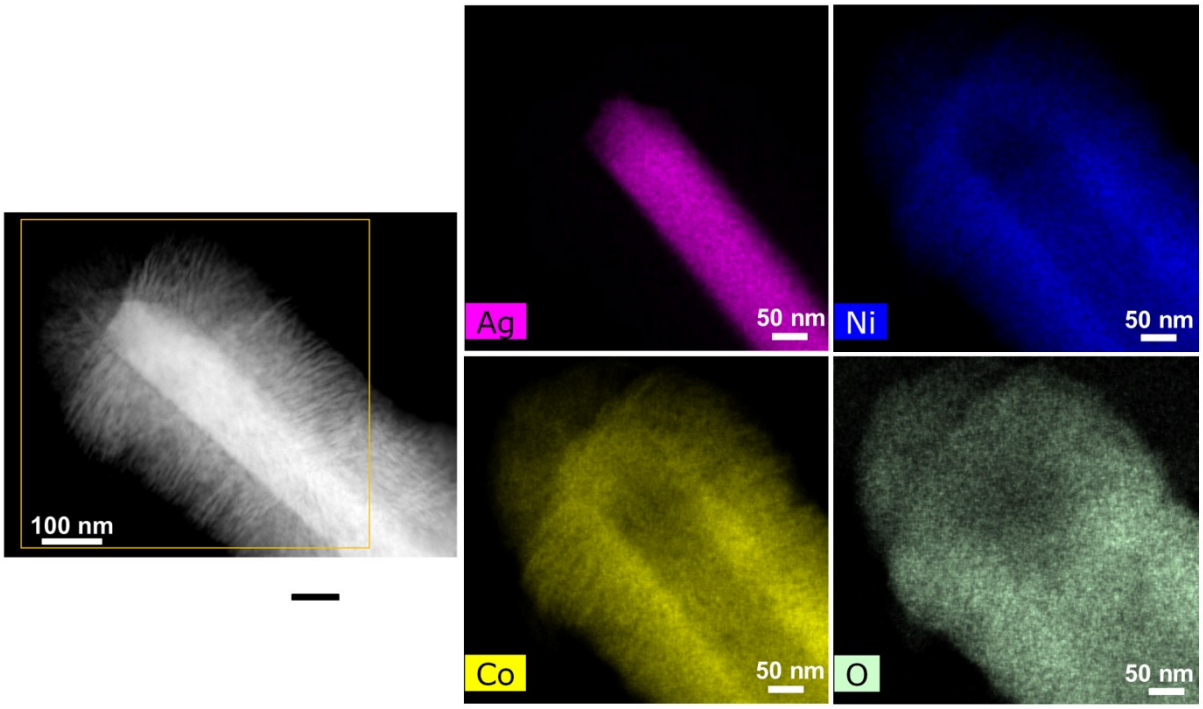

Figure S3. The HAADF-STEM image and the corresponding element distribution images in the selected yellow squares..

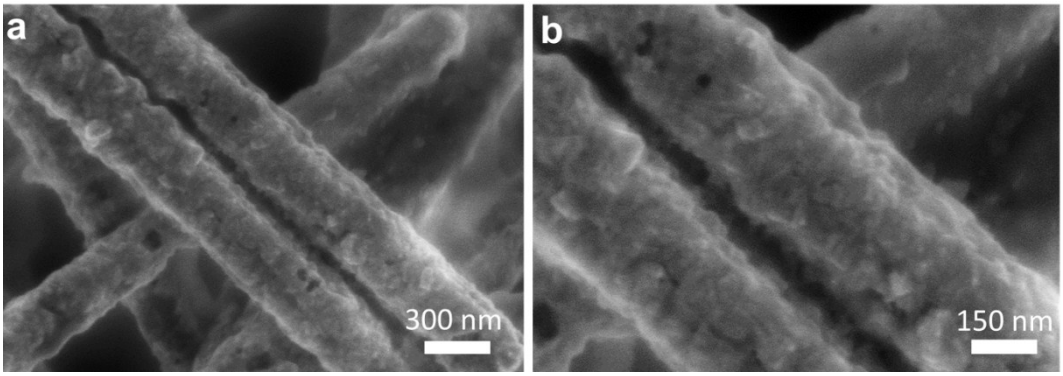

Figure S4. The high-magnification SEM images of Ni-Co@Ag NWs with different magnifications.

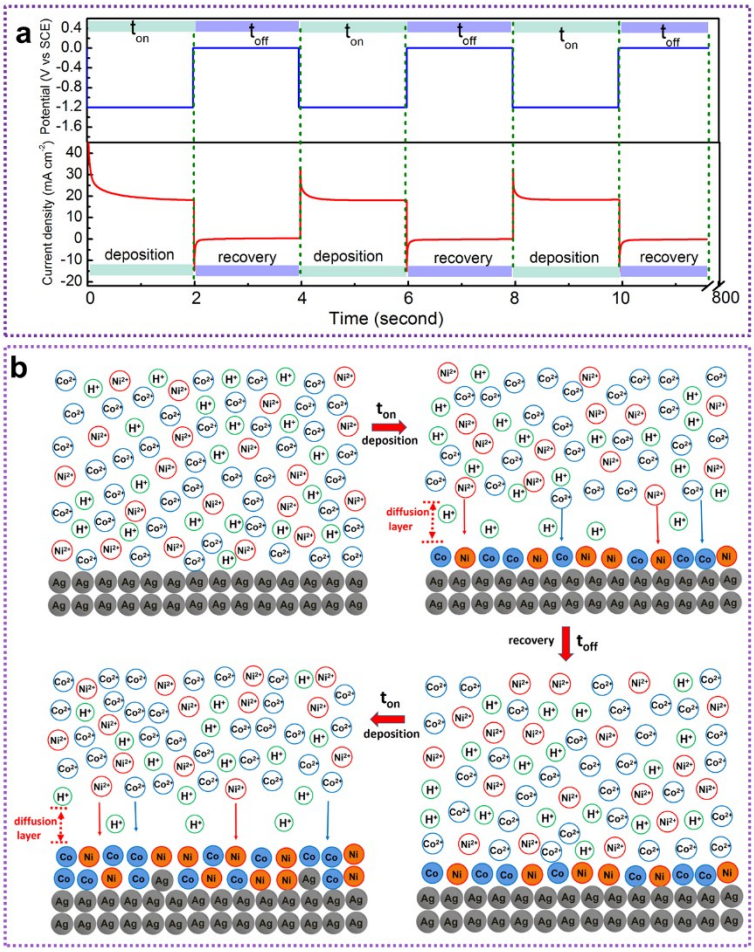

Figure S5. a) The pulsed potential electrodeposition model and b) the simplified electrochemical reaction mechanism for fabricating Ni-Co@Ag NWs.

In another aspect, the effect of hydrogen evolution can be minimized or avoided if the metal ions near deposition interfaces are being supplied sufficiently during the process of deposition. Here, pulsed potential electrodeposition model instead of potentiostatic electrodeposition model is used for depositing compact Ni-Co layer on Ag NWs (Figure S5a), in which a periodic potential delay process (t_{off}) is inserted between two successive deposition pulses. The sufficient t_{off} will allow the depleted metal ions near the deposition interface to be supplied sufficiently (Figure S5b), and the concentration of Co^{2+} and Ni^{2+} metal ions near deposition interfaces will recover before the next deposition pulse starts (Step (2)).[4, 5] Enough metal ions participating in the next deposition reaction will efficiently limit hydrogen evolution reaction(Step (3)).[1] In this case, the Ni-Co@Ag nanowires with a compact Ni-Co layer on Ag NWs are fabricated.

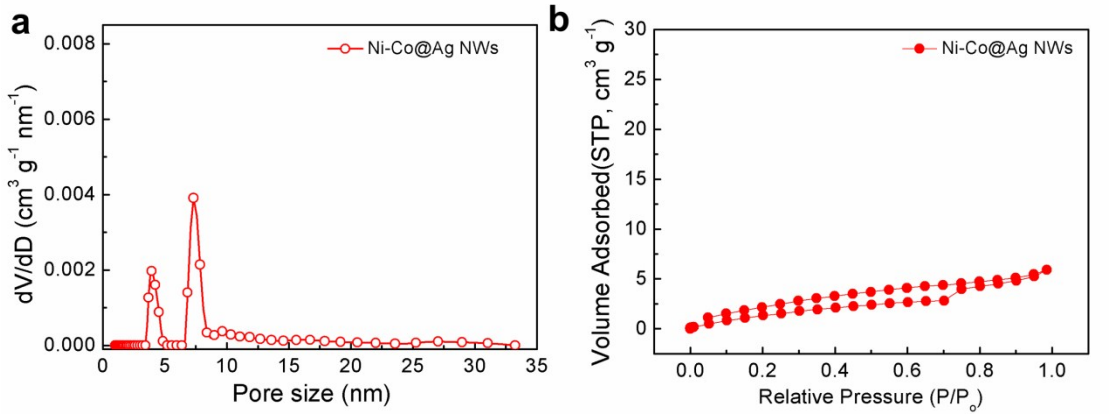

Figure S6. a) The pore-size distributions curves and b) the N_2 adsorption-desorption isotherms curves of Ni-Co@Ag NWs electrode.

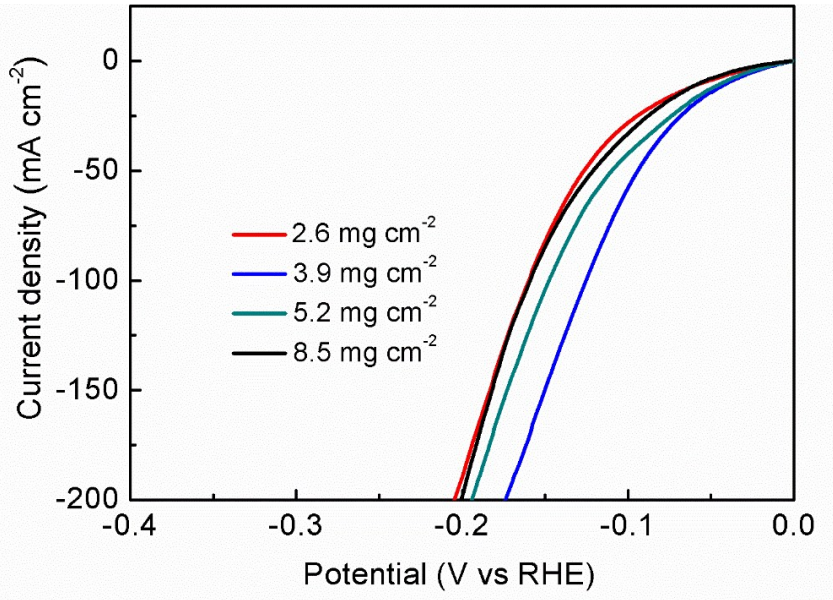

Figure S7. Polarization curves of the SIS Ni-Co@Ag NWs with the different mass loading on cloth fabric substrate for HER.

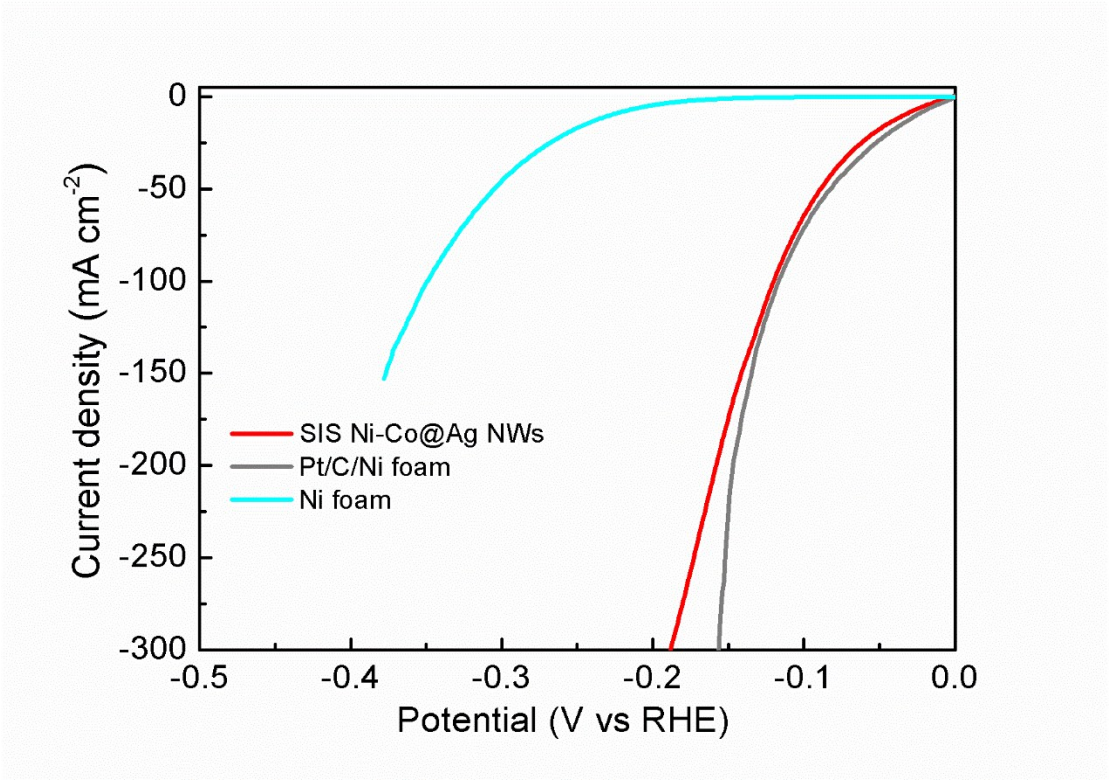

Figure S8. The polarization curves of SIS Ni-Co@Ag NWs for HER in contrast with that of Pt/C and Ni foam.

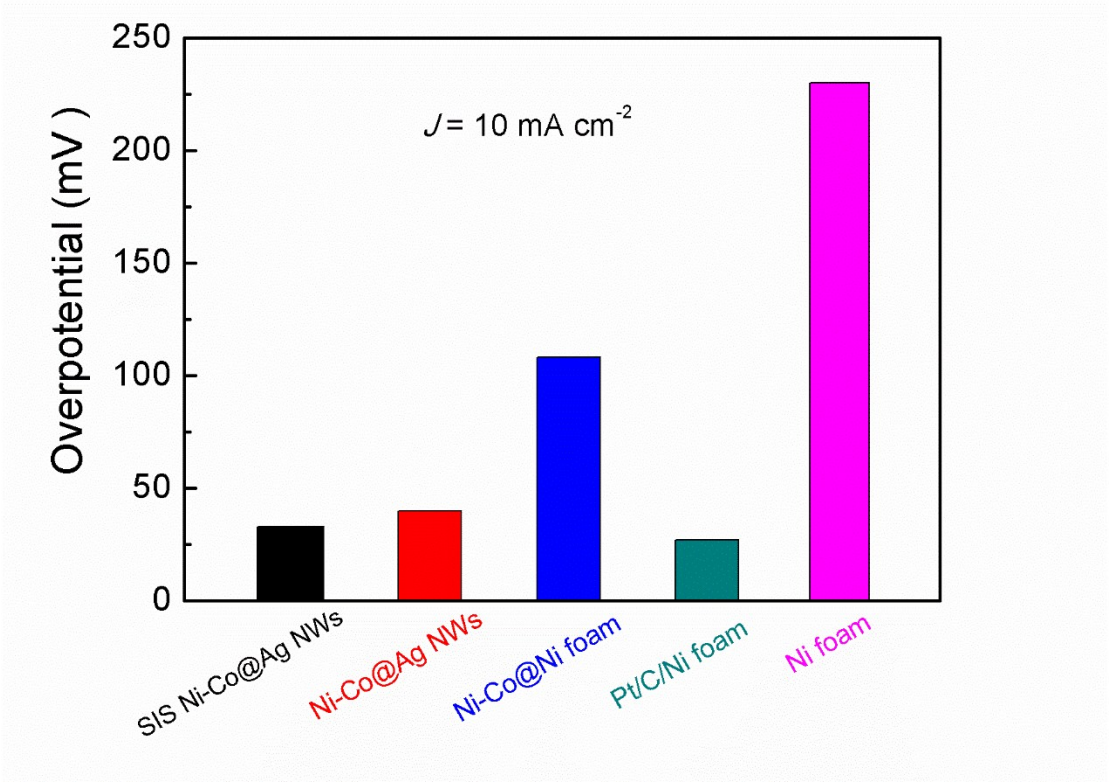

Figure S9. The overpotentials of different catalysts required to deliver a current density of $J = 10$ mA cm^{-2}.

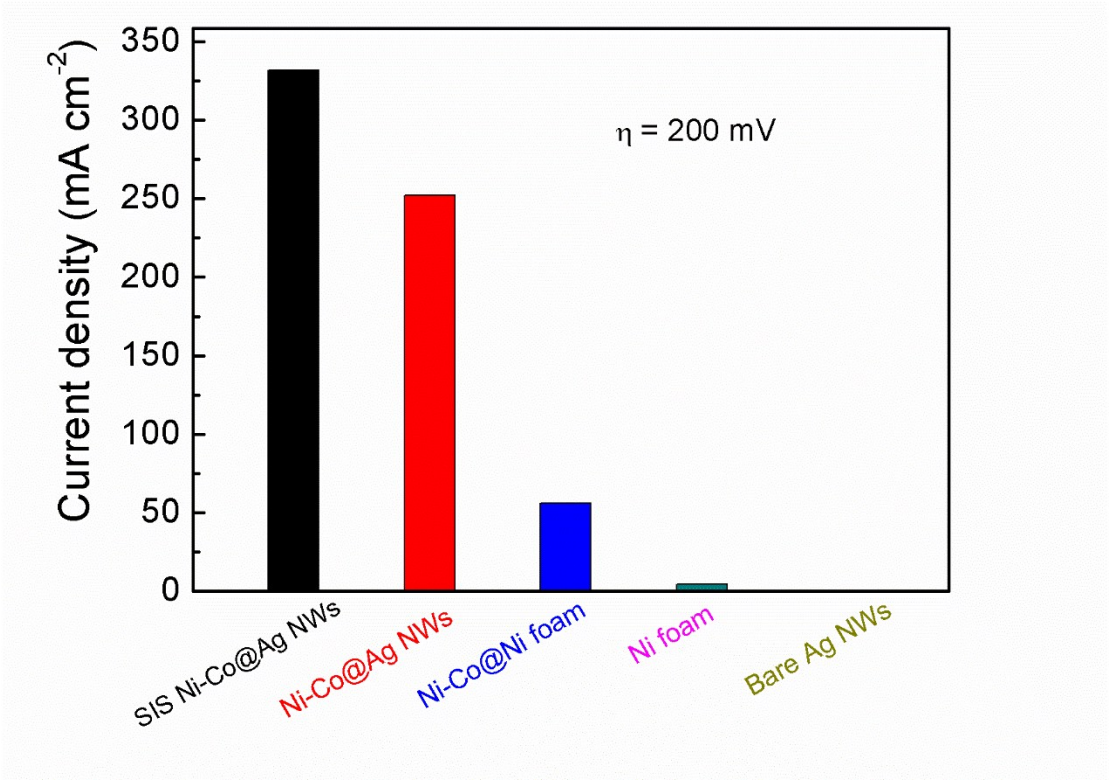

Figure S10. The corresponding current density of different catalysts at the overpotential of η = 200 mV.

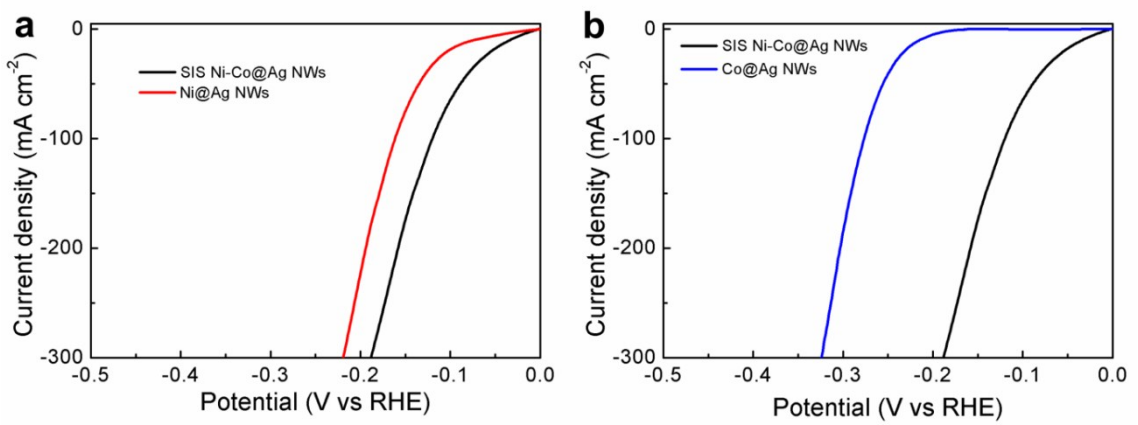

Figure S11. The polarization curves of SIS Ni-Co@Ag NWs in contrast with that of a) Ni@Ag NWs and b) Co@Ag NWs catalyst, respectively.

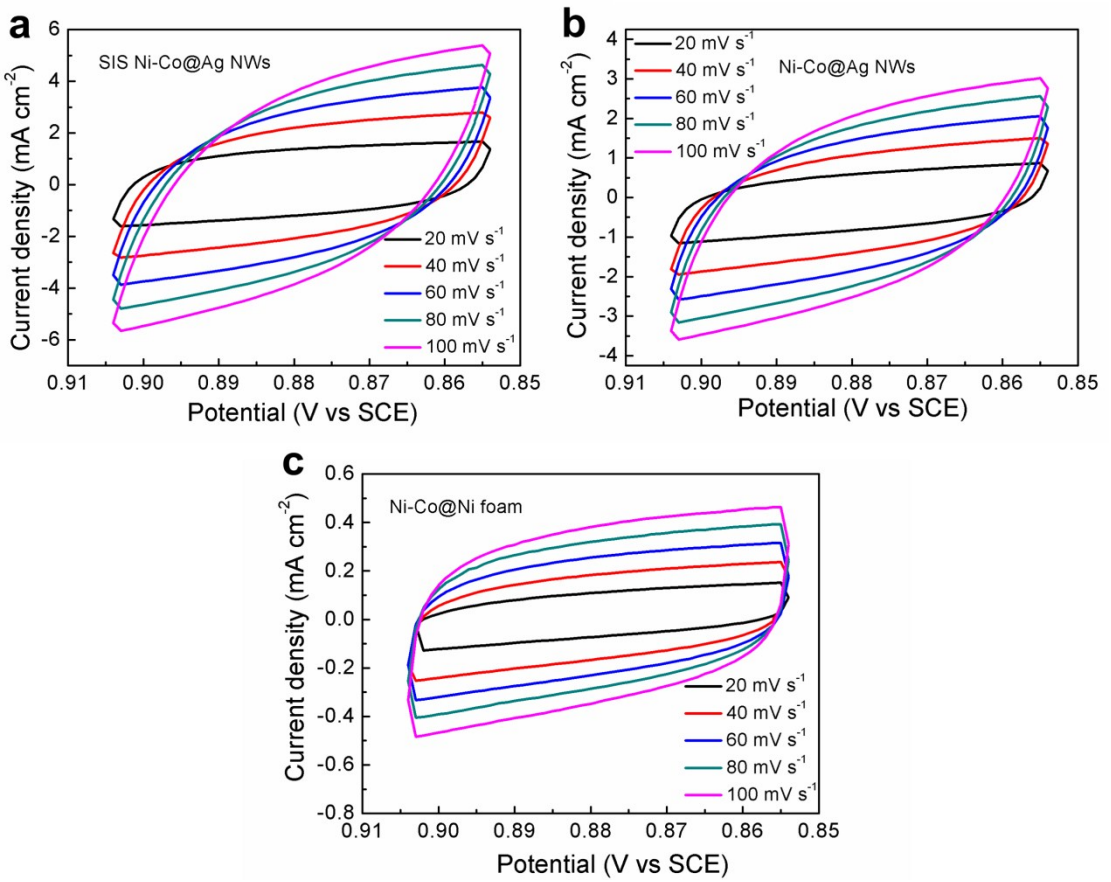

Figure S12. Cyclic voltammograms curves with different scan rates for electrochemical capacitance measurements of a) SIS Ni-Co@Ag NWs, b) Ni-Co@Ag NWs, c) Ni-Co@Ni foam electrodes.

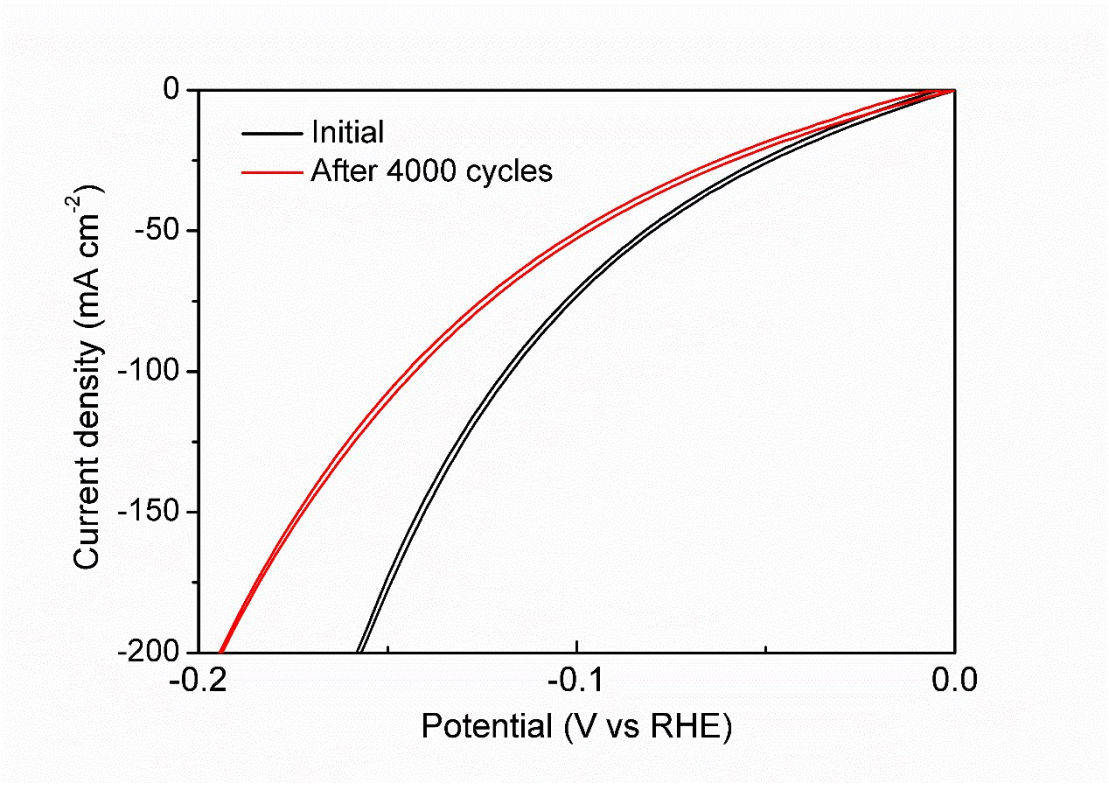

Figure S13. The CV LSV curves of SIS Ni-Co@Ag NWs at the initial and after 4000 CV cycles for HER recorded at forward scan and return scan, indicating little effect from the hysteresis.

Table S1. The elements distribution from EDS analysis for the bulk of SIS Ni-Co@Ag NWs catalyst and the elements proportion on the surface of catalyst quantified by the XPS survey.

Atomic Concentration (%)	Ag	Co	Ni	O
EDS analysis for the bulk of catalyst	13.13	47.43	37.58	1.86
XPS survey on the surface of catalyst	0.12	17.90	7.75	74.23

Table S2. BET surface area, pore volume, and average pore size of the SIS Ni-Co@Ag NWs and Ni-Co@Ag NWs samples.

Sample	BET surface area (m^2 g^{-1})	Pore volume (cm^3 g^{-1})	Average pore size (nm)
SIS Ni-Co@Ag NWs	24.587	0.042	5.572
Ni-Co@Ag NWs	4.435	0.009	6.083

Table S3. Performances comparison of SIS Ni-Co@Ag NWs with reported Ni-Co oxide-based catalysts for HER.

Electrocatalysts	Overpotential at 10 mA cm^{-2} (mV)	Tafel slop (mV dec^{-1})	Reference
SIS Ni-Co@Ag NWs	33	29	This work
$NiCo_2O_4$ holey nanosheets	260	127	*J. Am. Chem. Soc.* **2018**, 140, 5241.
$NiCo_2P_x$ nanowires	58	34	*Adv. Mater.* **2017**, 29, 1605502.
$NiCo_2S_4$ nanowire	210	59	*Adv. Funct. Mater*, **2016**, 26, 4661.
N-$NiCo_2S_4$ nanowire	41	37	*Nat. Commun.* **2018**, 9, 1425.
Ni-Co–P hollow nanobricks	107	46	*Energy Environ. Sci.* **2018**, 11, 872.
$Ni_{0.33}Co_{0.67}Se_2$	106	60	*Adv. Energy Mater.* **2017**, 7, 1602089
$Ni_{1-x}Co_xSe_2$ nanosheet	85	52	*Adv. Mater.* **2017**, 29, 1606521.
$NiCo_2O_4$ hollow microcuboids	110	50	*Angew. Chem.* **2016**, 128, 6398.
NiCo/$NiCoO_x$ heteronanostructures	155	35	*ACS Appl. Mater. Interfaces*, **2016**, 8, 3208.
$NiCoO_2$@C microflakes arrays	128	61	*Electrochim. Acta* **2018**, 284, 226.
NiCo–$NiCoO_2$@NC	94	125	*J. Mater. Chem. A* **2017**, 5, 15901.
$NiCo_2O_4$@NiO@ Ni Core/Shell nanocone array	120	58	*Part. Part. Syst. Charact.* **2017**, 34, 1700228.
Self-supported $NiCoO_2$ nanowires	101	42	*Nanoscale*, **2018**, 10, 18767.
Ni/Co mixed oxide nanocrystals	236	—	*Adv. Funct. Mater.* **2017**, 27, 1605121.
CFP/$NiCo_2O_4$/CuS	72	41	*Adv. Funct. Mater.* **2015**, 25, 6814.
CFP/$NiCo_2O_4$/$Co_{0.57}Ni_{0.43}$LMOs	52	34	*Nanoscale* **2016**, 8, 1390.

Table S4. Comparison of HER performances for SIS Ni-Co@Ag NWs with other reported nanowires based, bi- and tri-metal based electrocatalysts as well as others representative HER catalysts.

	Electrocatalysts	Overpotential at 10 mA cm^{-2} (mV)	Tafel slop (mV dec^{-1})	Reference
	SIS Ni-Co@Ag NWs	33	29	This work
Nanowire-based HER catalysts	CoP nanowire/CC	209	129	*J. Am. Chem. Soc.* **2014**, 136, 7587.
	FeP nanowire	194	75	*Chem. Commun.* **2016**, 52, 2819.
	Pt_3Ni_2-NWs-S/C	42	—	*Nat. Commun.* **2017**, 8, 14580.
	Cu nanowires @NiFe LDH	116	59	*Energy Environ.* Sci. **2017**, 10, 1820.
Bimetal based HER catalysts	$MoS_{2(1-x)}Se_{2x}/NiSe_2$	69	42	*Nat. Commun.* **2016**, 7, 12765.
	CoMoP@C	81	55	*Energy Environ. Sci.* **2017**, 10, 788.
	$NiMo_3S_4$	257	98	*Angew. Chem. Int. Ed.* **2016**, 55, 15240.
	NiFe LDH/NF	210	—	*Science* **2014**, 345, 1593.
Other typical HER catalysts	$Ni(OH)_2$/ Pt-islands/ Pt(111)	138	—	*Science* **2011**, 334, 1256
	NiO/Ni-CNT	80	51	*Nat. Commun.* **2014**, 5: 4695.
	CoS_2/RGO-CNT	142	51	*Angew. Chem. Int. Ed.* **2014**, 126, 12802.
	Pt-Ni multipods	65	74	*Nat. Commun.* **2017**, 8, 15131.

Table S5. The adsorption enthalpies of hydrogen and water molecule on 5 considered sites A, B, C, D and E of NiCo/NiCoO and NiCo/NiCoO@Ag electrodes.

H Adsorption Enthalpy (eV)	Ni	Co	Hollow	O	Co-hollow
Site	A	B	C	D	E
NiCo/NiCoO	-0.3025	-0.5645	-0.5855	-0.1015	-0.9525
NiCo/NiCoO@Ag	-0.5235	-0.2965	-0.4625	-0.0655	-0.8435

H_2O Adsorption Enthalpy (eV)	Ni	Co	Hollow	O	Co-hollow
Site	A	B	C	D	E
NiCo/NiCoO	-0.108	-0.412	-0.576	-0.373	-0.041
NiCo/NiCoO@Ag	-0.141	-0.488	-0.726	-0.383	0.061

References

1. K. Nielsch, F. Müller, A. P. Li and U. Gösele, *Adv. Mater.*, 2000, **12**, 582.
2. P.-C. Hsu, S.-K. Seol, T.-N. Lo, C.-J. Liu, C.-L. Wang, C.-S. Lin, Y. Hwu, C. H. Chen, L.-W. Chang, J. H. Je and G. Margaritondo, *J. Electrochem. Soc.*, 2008, **155**, D400.
3. H. C. S. And and M. Liu, *Chem. Mater.*, 2004, **16**, 5460.
4. A. R. Despic and K. I. Popov, *J. Appl. Electrochem.*, 1971, **1**, 275.
5. H. Natter, M. Schmelzer and R. Hempelmann, *J. Mater. Res.*, 1998, **13**, 1186.